





Solitonic model of the condensate

Andrey Gelash ^{1,2,*}, Dmitry Agafontsev ^{2,3}, Pierre Suret ^{4,5} and Stéphane Randoux ^{4,5}

¹*Institute of Automation and Electrometry SB RAS, Novosibirsk 630090, Russia*

²*Skolkovo Institute of Science and Technology, Moscow 121205, Russia*

³*P. P. Shirshov Institute of Oceanology of RAS, 117997, Moscow, Russia*

⁴*Univ. Lille, CNRS, UMR 8523 - PhLAM—Physique des Lasers Atomes et Molécules, F-59000 Lille, France*

⁵*Centre d'Etudes et de Recherches Lasers et Applications (CERLA), 59655 Villeneuve d'Ascq, France*



(Received 16 May 2021; accepted 13 October 2021; published 27 October 2021)

We consider a spatially extended box-shaped wave field that consists of a plane wave (the condensate) in the middle and equals zero at the edges, in the framework of the focusing one-dimensional nonlinear Schrödinger equation. Within the inverse scattering transform theory, the scattering data for this wave field is presented by the continuous spectrum of the nonlinear radiation and the soliton eigenvalues together with their norming constants; the number of solitons N is proportional to the box width. We remove the continuous spectrum from the scattering data and find analytically the specific corrections to the soliton norming constants that arise due to the removal procedure. The corrected soliton parameters correspond to symmetric in space N -soliton solution, as we demonstrate analytically in the paper. Generating this solution numerically for N up to 1024, we observe that, at large N , it converges asymptotically to the condensate, representing its solitonic model. Our methods can be generalized for other strongly nonlinear wave fields, as we demonstrate for the hyperbolic secant potential, building its solitonic model as well.

DOI: [10.1103/PhysRevE.104.044213](https://doi.org/10.1103/PhysRevE.104.044213)

I. INTRODUCTION

The focusing one-dimensional nonlinear Schrödinger equation (1D-NLSE),

$$i\psi_t + \frac{1}{2}\psi_{xx} + |\psi|^2\psi = 0, \quad (1)$$

where t is time, x is spatial coordinate, and ψ is a complex wave field, is a universal model of nonlinear physics, describing the evolution of a narrow-band signal in weakly nonlinear media. As such, it is widely applicable in different fields of studies ranging from nonlinear optics to hydrodynamics and Bose-Einstein condensates [1–3]. The simplest solution of Eq. (1) is a plane wave (also called the condensate), which appears as a background in various nonlinear processes, such as development of the modulational instability, propagation of breatherlike structures, and formation of rogue waves [2,4–6]. The condensate of unit amplitude can be simply written as $\psi_c = e^{it}$; it is modulationally unstable with respect to long-wave harmonic perturbations having wave vectors $k \in (-2, 2)$. At the linear stage of the modulation instability (MI), the perturbations grow as $\propto e^{\gamma t}$, where γ is the well-known MI growth rate [7,8]:

$$\gamma = |k| \sqrt{1 - k^2/4}. \quad (2)$$

From a mathematical point of view, the 1D-NLSE belongs to a remarkable class of the so-called integrable systems, as it can be integrated using the inverse scattering transform

(IST) technique [9–11]. Specifically, the 1D-NLSE allows transformation to the so-called *scattering data*, which is in one-to-one correspondence with the wave field and, similarly to the Fourier harmonics in the linear wave theory, changes trivially during the motion. Transformation to the scattering data includes calculation of the eigenvalue spectrum for specific auxiliary linear systems, in which the wave field of the 1D-NLSE plays the role of the potential. For spatially localized wave fields, the eigenvalue spectrum contains the discrete (solitons) and continuous (nonlinear dispersive waves or nonlinear radiation) parts. In contrast to the linear wave theory, where the arithmetic sum of Fourier harmonics constitutes the wave field, the scattering data reconstructs it via the nonlinear system of integral Gelfand-Levitan-Marchenko (GLM) equations. In the pure solitonic case, these equations can be solved analytically to the exact formulas describing multi-soliton solutions.

In the limit of weak nonlinearity (small-amplitude waves), the solitonic part of the scattering data vanishes and the remaining continuous spectrum coincides at the leading order with the Fourier spectrum of the wave field [3]. On the other hand, when nonlinearity is substantial, solitons should dominate the dynamics [9], which is currently under active investigation in nonlinear optics and hydrodynamics, see, e.g., Refs. [12–17]. Additionally, a rapidly developing area of theoretical and experimental research on the statistics of integrable systems with random input, called, in general, *integrable turbulence* [18], brings to the agenda the fundamental question concerning the role of solitons in shaping the major statistical characteristics of the wave field, such as the wave-action spectrum and distribution of intensity [19–26].

*agelash@gmail.com

For the 1D-NLSE, the condensate solution represents one of the most well-known examples of strongly nonlinear wave fields. In the present paper, we build its solitonic model, that describes the condensate asymptotically at large number of solitons. The idea of leaving only the solitonic part of the wave field comes from a recent study [26], where it has been demonstrated numerically that the modulationally unstable condensate, at its long-time statistically stationary state, can be accurately modeled (in the statistical sense) with a dense bound-state soliton gas designed to follow the solitonic structure of the condensate. Here we develop this idea further and establish an analytical correspondence between the condensate at the initial time and specific multisoliton solution. We believe that, in the solitons-only approximation, this correspondence will provide access to analytical description of various nonlinear phenomena developing on the condensate background, e.g., development of the modulational instability, propagation of breatherlike structures, and formation of rogue waves, and we are going to explore this line of research in the near future.

As a model of the condensate, we consider a spatially extended box-shaped (rectangular) wave field that consists of a plane wave in the middle and equals zero at the edges [see Eq. (23) below], similar to some laboratory experiments, see, e.g., Refs. [25,27]. For this model, the scattering data is known analytically within the IST theory [28]: it contains both the continuous (nonlinear radiation) and discrete (solitons) parts of eigenvalue spectrum, with the number of solitons proportional to the box width. We remove the continuous spectrum from the scattering data and find analytically the specific corrections to the soliton norming constants that arise due to the removal procedure; the necessity for such corrections is explained in Sec. IV. The corrected soliton parameters correspond to multisoliton solution that is symmetric in space, as we demonstrate analytically. Generating this solution numerically for the number of solitons N of up to 1024, we observe that it is similar to the initial box-shaped wave field, but contains residual oscillations as a manifestation of the Gibbs-like phenomenon. These oscillations have finite amplitude at the edges, but are small in a broad central region, so our solitonic model converges asymptotically to the condensate at large number of solitons (or, equivalently, at large box width).

Note that wave fields, consisting of a large number of solitons and often called soliton gases, may have various configurations characterized by different soliton amplitudes, velocities, and spatial densities with all these quantities being random. While rarefied soliton gas can be modelled straightforwardly with two-soliton interaction formulas [29], perturbation theory [30,31], and adiabatic approximation [32–34], the case of a dense soliton gas requires usage of exact multisoliton solutions obtained via IST techniques [24,26,35], as we apply in the present paper.

The paper is organized as follows. In the next section, we give a brief overview of the IST theory in relation to the 1D-NLSE model. In Sec. III, we recall the scattering data of the box potential. In Sec. IV, we remove the continuous spectrum component and find analytically the specific corrections to the soliton norming constants. In Sec. V, we study—both analytically and numerically—the multisoliton solution corresponding to the corrected soliton parameters.

The last two Secs. VI and VII, contain discussions and conclusions, respectively. The paper also has several Appendices, where we study the constructed multisoliton solution in more detail and provide some calculations related to corrections of the soliton norming constants. Additionally, in Appendix C, we build solitonic model for the hyperbolic secant potential, demonstrating that our methods can be generalized straightforwardly for other strongly nonlinear wave fields.

II. THE IST AND MULTI-SOLITON SOLUTIONS

A. The IST formalism

Formulation of the scattering problem for the 1D-NLSE (1) starts from introduction of the following auxiliary Zakharov-Shabat (ZS) linear system for the two-component vector wave function $\Phi(x, t, \lambda) = (\phi_1, \phi_2)^T$, see Ref. [9]:

$$\Phi_x = \begin{pmatrix} -i\lambda & \psi \\ -\psi^* & i\lambda \end{pmatrix} \Phi, \quad (3)$$

$$\Phi_t = \begin{pmatrix} -i\lambda^2 + \frac{i}{2}|\psi|^2 & \lambda\psi + \frac{i}{2}\psi_x \\ -\lambda\psi^* + \frac{i}{2}\psi_x^* & i\lambda^2 - \frac{i}{2}|\psi|^2 \end{pmatrix} \Phi, \quad (4)$$

from which the 1D-NLSE is obtained as compatibility condition

$$\Phi_{xt} = \Phi_{tx}.$$

Here $\lambda = \xi + i\eta$ is complex-valued spectral parameter and the star stands for the complex conjugate.

The first equation of the ZS system can be rewritten in the form of the eigenvalue problem for the spectral parameter λ :

$$\widehat{\mathcal{L}}\Phi = \lambda\Phi, \quad \widehat{\mathcal{L}} = i \begin{pmatrix} 1 & 0 \\ 0 & -1 \end{pmatrix} \frac{\partial}{\partial x} - i \begin{pmatrix} 0 & \psi \\ \psi^* & 0 \end{pmatrix}. \quad (5)$$

For each solution $\Phi(x, t, \lambda) = (\phi_1, \phi_2)^T$, corresponding to an eigenvalue λ , there exists a counterpart $\widetilde{\Phi}(x, t, \lambda^*) = (-\phi_2^*, \phi_1^*)^T$ corresponding to the complex-conjugate eigenvalue λ^* . Thus, without loss of generality, we consider the spectral parameter in the upper half of the complex plane only, $\eta = \text{Im } \lambda \geq 0$.

Similarly to quantum mechanics, see, e.g., Ref. [36], the scattering problem (5) for the wave function Φ is introduced on the real line $\lambda = \xi$ ($\xi \in \mathbb{R}$) with the following asymptotics at infinity (the so-called right scattering problem, in contrast to the left scattering problem; see, e.g., Ref. [37]):

$$\lim_{x \rightarrow -\infty} \left\{ \Phi - \begin{pmatrix} e^{-i\xi x} \\ 0 \end{pmatrix} \right\} = 0, \quad (6)$$

$$\lim_{x \rightarrow +\infty} \left\{ \Phi - \begin{pmatrix} a e^{-i\xi x} \\ b e^{i\xi x} \end{pmatrix} \right\} = 0. \quad (7)$$

In this problem, the wave field ψ of the 1D-NLSE is considered as a potential for the scattering wave Φ , while a and b represent the scattering coefficients satisfying

$$a(\xi)a(\xi)^* + b(\xi)b(\xi)^* = 1. \quad (8)$$

In the present paper, we consider only wave fields belonging to the Schwartz space, i.e., that are spatially localized and rapidly decaying. In this case, the eigenvalues λ of the ZS system are usually presented by a finite number of discrete points λ_n (discrete spectrum) with $\eta_n = \text{Im } \lambda_n > 0$, $n = 1, \dots, N$, and the real line $\lambda = \xi \in \mathbb{R}$ (continuous spectrum), see Ref. [9].

Note that there are some exceptions when wave fields from the Schwartz space are characterized by an infinite number of eigenvalues, see Ref. [38], that is not the case for this work.

The coefficient $a(\xi)$ can be analytically continued to the upper half of the λ plane as a function $a(\lambda)$ having simple zeros at the eigenvalue points, $a(\lambda_n) = 0$ (we do not consider the degenerate case when an eigenvalue point represents a multiple zero). In addition to the real line $\lambda = \xi$, the coefficient b can also be defined, in general, only at the eigenvalue points λ_n . However, it can be analytically continued to the whole upper half-plane if the potential ψ has a compact support [39]. Bounded solutions (6) and (7) exist for real-valued spectral parameter, $\lambda = \xi$, and also for complex-valued λ , $\eta = \text{Im } \lambda > 0$, if and only if $a(\lambda) = 0$.

The full set of the scattering data represents a combination of the discrete $\{\lambda_n, \rho_n\}$ and continuous $\{r\}$ spectra,

$$\begin{aligned} & \{\lambda_n \mid a(\lambda_n) = 0, \text{Im } \lambda_n > 0\}, \\ \rho_n &= \frac{b(\lambda_n)}{a'(\lambda_n)}, \quad r(\xi) = \frac{b(\xi)}{a(\xi)}, \end{aligned} \quad (9)$$

where $a'(\lambda)$ is complex derivative of $a(\lambda)$, ρ_n are the so-called norming constants associated with the eigenvalues λ_n , and $r(\xi)$ is the reflection coefficient defined at the real line $\xi \in \mathbb{R}$. Most importantly, the time evolution of the scattering data (9) is trivial,

$$\begin{aligned} \forall n : \lambda_n &= \text{const}, \\ \rho_n(t) &= \rho_n(0)e^{2i\lambda_n^2 t}, \\ r(\xi, t) &= r(\xi, 0)e^{2i\xi^2 t}, \end{aligned} \quad (10)$$

and the wave field ψ can be recovered with the IST by solving the integral GLM equations [10]. Note, however, that in the general case the latter procedure can only be done numerically, asymptotically at $t \rightarrow \pm\infty$, or in the semiclassical approximation, see, e.g., Refs. [40,41].

The reflection coefficient $r(\xi)$ corresponds to nonlinear dispersive waves, while the discrete eigenvalues λ_n together with the norming constants ρ_n correspond to solitons. In particular, for $n = 1, \dots, N$, the eigenvalues $\lambda_n = \xi_n + i\eta_n$ contain information about the soliton amplitudes, $A_n = 2\eta_n$, and group velocities, $V_n = -2\xi_n$, while the soliton norming constants—about their positions in space $x_n^{(\text{IST})} \in \mathbb{R}$ and complex phases $\theta_n^{(\text{IST})} \in [0, 2\pi)$, see Ref. [37]:

$$\rho_n = -iA_n \exp[-2i\lambda_n x_n^{(\text{IST})} - i\theta_n^{(\text{IST})}]. \quad (11)$$

Here the IST superscripts designate that the positions and phases are written for the IST formalism, in contrast to the DM formalism, which we will discuss below. Note that $x_n^{(\text{IST})}$ and $\theta_n^{(\text{IST})}$ equal to the observed in the physical space position and phase of a soliton only for the one-soliton solution,

$$\begin{aligned} \psi_{(1)}(x, t) &= A_1 \frac{\exp[iV_1(x - x_1^{(\text{IST})}) + i\theta_1^{(\text{IST})}]}{\cosh A_1(x - x_1^{(\text{IST})})}, \\ x_1^{(\text{IST})} &= x_{10}^{(\text{IST})} + V_1 t, \\ \theta_1^{(\text{IST})} &= \theta_{10}^{(\text{IST})} + \frac{1}{2}(A_1^2 + V_1^2)t, \end{aligned}$$

where $x_{10}^{(\text{IST})}$ and $\theta_{10}^{(\text{IST})}$ are the position and phase at $t = 0$. In the presence of other solitons or dispersive waves, the observed position and phase of a soliton may differ considerably from $x_n^{(\text{IST})}$ and $\theta_n^{(\text{IST})}$.

For the reflectionless case $r(\xi) = 0$, the dispersive waves are absent and the IST procedure can be performed analytically, leading to an exact N -soliton solution (N -SS) $\psi_{(N)}(x, t)$ which we write in the following form, see Refs. [10,42]:

$$\begin{aligned} \psi_{(N)}(x, t) &= -2i\rho_k^*(t)e^{-i\lambda_k^* x} \{[\mathbf{E} + \mathbf{B}^*(x, t)\mathbf{B}(x, t)]^{-1}\}_{k,j} \\ &\quad \times e^{-i\lambda_j^* x}. \end{aligned} \quad (12)$$

Here $k, j = 1, \dots, N$ are summation indexes, \mathbf{E} is $N \times N$ unit matrix, and \mathbf{B} is $N \times N$ matrix with elements

$$\mathbf{B}_{k,j}(x, t) = i\rho_j(t)(\lambda_k^* - \lambda_j)^{-1}e^{-i(\lambda_k^* - \lambda_j)x}. \quad (13)$$

B. The dressing method formalism

An alternative to the IST procedure for construction of a N -SS is the so-called dressing method (DM) [10,43], also known as the Darboux transformation [44,45]. The DM allows us to add solitons to the resulting solution recursively one at a time using special algebraic construction [10,43,45]. The numerical implementation of the DM turns out to be much more stable than the IST approach (12) that allows us to use it for computing multisoliton wave fields [24].

The dressing procedure starts from the trivial potential of the 1D-NLSE, $\psi_{(0)}(x) = 0$ for $x \in \mathbb{R}$, and the corresponding matrix solution of the ZS system (3),

$$\Phi^{(0)}(x, \lambda) = \begin{pmatrix} e^{-i\lambda x} & 0 \\ 0 & e^{i\lambda x} \end{pmatrix}; \quad (14)$$

here we fix time, $t = 0$, for definiteness. At the n th step of the recursive method, the n -soliton potential $\psi_{(n)}(x)$ is constructed via the $(n - 1)$ -soliton potential $\psi_{(n-1)}(x)$ and the corresponding matrix solution $\Phi^{(n-1)}(x, \lambda)$ as

$$\psi_{(n)}(x) = \psi_{(n-1)}(x) + 2i(\lambda_n - \lambda_n^*) \frac{q_{n1}^* q_{n2}}{|\mathbf{q}_n|^2}, \quad (15)$$

where vector $\mathbf{q}_n = (q_{n1}, q_{n2})^T$ is determined by $\Phi^{(n-1)}(x, \lambda)$ and the scattering data of the n th soliton $\{\lambda_n, C_n\}$:

$$\mathbf{q}_n(x) = [\Phi^{(n-1)}(x, \lambda_n^*)]^* \begin{pmatrix} 1 \\ C_n \end{pmatrix}. \quad (16)$$

Here $C_n, n = 1, \dots, N$, are the soliton norming constants in the DM formalism, see the discussion below. The corresponding matrix solution $\Phi^{(n)}(x, \lambda)$ of the ZS system is calculated via the so-called dressing matrix $\sigma^{(n)}(x, \lambda)$,

$$\Phi^{(n)}(x, \lambda) = \sigma^{(n)}(x, \lambda)\Phi^{(n-1)}(x, \lambda), \quad (17)$$

$$\sigma_{ml}^{(n)}(x, \lambda) = \delta_{ml} + \frac{\lambda_n - \lambda_n^* q_{nm}^* q_{nl}}{\lambda - \lambda_n} \frac{q_{nm}^* q_{nl}}{|\mathbf{q}_n|^2}, \quad (18)$$

where $m, l = 1, 2$ and δ_{ml} is the Kronecker delta. The time dependency is recovered using the time evolution of the norming constants,

$$C_n(t) = C_n(0)e^{-2i\lambda_n^2 t}, \quad (19)$$

and repeating the DM for each moment of time.

The outcome of the DM for a N -SS can be written as a ratio of two determinants,

$$\psi_{(N)}(x, t) = -2i \frac{\det \tilde{\mathbf{M}}}{\det \mathbf{M}}, \quad M_{kj} = \frac{(\tilde{\mathbf{q}}_k \cdot \tilde{\mathbf{q}}_j^*)}{\lambda_k - \lambda_j^*},$$

$$\tilde{\mathbf{M}} = \begin{pmatrix} 0 & \tilde{q}_{1,2} & \cdots & \tilde{q}_{N,2} \\ \tilde{q}_{1,1}^* & & & \\ \vdots & & \mathbf{M}^T & \\ \tilde{q}_{N,1}^* & & & \end{pmatrix}, \quad (20)$$

where we use the new two-component vectors $\tilde{\mathbf{q}}_n$,

$$\tilde{\mathbf{q}}_n(x, t) = \begin{pmatrix} \tilde{q}_{n,1} \\ \tilde{q}_{n,2} \end{pmatrix} = \begin{pmatrix} C_n^{-1/2} e^{i\lambda_n x} \\ C_n^{1/2} e^{-i\lambda_n x} \end{pmatrix},$$

and the dot in $(\tilde{\mathbf{q}}_k \cdot \tilde{\mathbf{q}}_j^*) = \tilde{q}_{k,1} \tilde{q}_{j,1}^* + \tilde{q}_{k,2} \tilde{q}_{j,2}^*$ means the real-symmetric vector scalar product. The DM norming constants C_n are related to the IST norming constants ρ_n as follows, see Refs. [42,46]:

$$\rho_n(t) = \frac{1}{C_n(t)} \prod_{k=1}^N (\lambda_n - \lambda_k^*) \times \prod_{j \neq n}^N \frac{1}{\lambda_n - \lambda_j}. \quad (21)$$

Note that this equation is valid for pure multisoliton solutions only.

Within the DM formalism, the norming constants C_n contain information about soliton positions $x_n^{(\text{DM})}$ and phases $\theta_n^{(\text{DM})}$:

$$C_n = -\exp[2i\lambda_n x_n^{(\text{DM})} + i\theta_n^{(\text{DM})}]. \quad (22)$$

These parameters do not coincide in the general case with the IST positions $x_n^{(\text{IST})}$ and phases $\theta_n^{(\text{IST})}$, since the IST is built on a nonsymmetric formulation of the scattering problems (6) and (7), while the DM is symmetric by construction, see, e.g., Refs. [43,45]. Similar to the IST formalism, $x_n^{(\text{DM})}$ and $\theta_n^{(\text{DM})}$ are equal to the observed physical space position and phase of a soliton, but only for the one-soliton solution; in the presence of other solitons or dispersive waves, the observed position and phase may differ considerably from $x_n^{(\text{DM})}$ and $\theta_n^{(\text{DM})}$.

Equations (12) and (20) represent the exact same multisoliton solution, in which the soliton norming constants ρ_n (for the IST formalism) and C_n (for the DM formalism) are parameterized in a different way, with the relation (21) connecting the two parametrizations. In the present paper, we need both parametrizations. In particular, to construct the wave field for a multisoliton solution, we need the DM as it is much more stable numerically, see Ref. [24] for details. On the other hand, to our knowledge, a procedure that would allow us to calculate the scattering data in the DM formalism directly from the wave field, without solving the ZS system in the IST formalism and the subsequent transition to the DM formalism, has not been developed yet. For these reasons, we start with the scattering data in the IST formalism, then remove the nonlinear radiation and calculate the specific corrections to the soliton norming constants and, finally, perform transition to the DM formalism and construct the wave field for the corresponding multisoliton solution numerically.

III. SCATTERING DATA FOR THE BOX POTENTIAL

We model the condensate with a box (rectangular) potential of unit amplitude and width L :

$$\psi(x) = \begin{cases} 1, & |x| \leq L/2 \\ 0, & |x| > L/2. \end{cases} \quad (23)$$

For real spectral parameter $\lambda = \xi \in \mathbb{R}$, the scattering coefficients for this wave field can be found in the following closed form [28]:

$$a(\xi) = e^{iL\xi} \left\{ \cos(\chi L) - i\xi \frac{\sin(\chi L)}{\chi} \right\}, \quad (24)$$

$$b(\xi) = -\sin(\chi L)/\chi, \quad (25)$$

where

$$\chi = \sqrt{1 + \xi^2},$$

so the reflection coefficient is written as

$$r(\xi) = -\frac{e^{-i\xi L} \sin(L\chi)}{\chi \cos(L\chi) - i\xi \sin(L\chi)}. \quad (26)$$

The scattering coefficients can be analytically continued to the upper half-plane by replacement $\xi \rightarrow \lambda$; for the coefficient b , this is possible since the box potential has compact support $x \in [-L/2, L/2]$. The condition $a(\lambda) = 0$ leads to transcendental equation defining the soliton eigenvalues:

$$\cos(L\sqrt{1 + \lambda^2}) - \frac{i\lambda}{\sqrt{1 + \lambda^2}} \sin(L\sqrt{1 + \lambda^2}) = 0. \quad (27)$$

For $\eta = \text{Im } \lambda > 0$, Eq. (27) has N simple discrete roots λ_n , representing the solitonic structure of the box-shaped wave field (23); here

$$N = \text{integer}[L/\pi + 1/2]. \quad (28)$$

These roots lie on the imaginary axis in the interval $(0, i)$, see Refs. [47–49],

$$\left\{ \{\lambda_n\} = \{i\eta_n\} \mid \tan(L\sqrt{1 - \eta_n^2}) = -\frac{\sqrt{1 - \eta_n^2}}{\eta_n}, \right.$$

$$\left. 0 < \eta_n < 1, \quad n = 1, \dots, N \right\}, \quad (29)$$

meaning that the solitons of the box potential have zero velocities, $V_n = -2 \text{Re } \lambda_n = 0$. Here and below we assume that the eigenvalues are sorted in *descending* order, $\eta_m < \eta_l$ for $m > l$.

When the box width L increases, the number of solitons N changes discretely according to Eq. (28), with the N th soliton emerging at $L = \pi(N - 1/2)$. Hence, the box width can be parameterized as

$$L = L_N + \Delta L, \quad L_N = \pi(N - 1/2), \quad \Delta L \in [0, \pi), \quad (30)$$

meaning that the number of solitons N remains constant until the next jump by one soliton at $L = L_N + \pi$. Note that for $L \gg 1$, the ZS scattering problem can be solved within the semiclassical approach, leading to an approximate formula for the soliton eigenvalues [40]:

$$\lambda_n^{(\text{sc})} = i\sqrt{1 - \left[\frac{\pi(n - 1/2)}{L} \right]^2}. \quad (31)$$

The soliton norming constants in the IST formalism can be computed from the definition (9) using the transcendental condition (29),

$$\rho_n = \frac{e^{\eta_n L} (1 - \eta_n^2)}{i(1 + \eta_n L)}, \quad (32)$$

that completes the full set of the scattering data for the box potential (23).

IV. REMOVAL OF THE NONLINEAR RADIATION

Without nonlinear radiation, when only one soliton is present, its observed physical position in space and its phase coincide with the corresponding IST parameters (11) obtained from the solution of the ZS system (5). For definiteness, we place a single soliton with eigenvalue $\lambda_n = \xi_n + i\eta_n$ far away to the left of the coordinate origin $x = 0$. Let us now add to the wave field a localized nonlinear radiation near $x = 0$ which does not have solitonic content. The soliton and radiation practically do not interact in the physical space as both structures are localized, so we can construct the soliton-and-radiation potential as arithmetic sum of the soliton-only and radiation-only potentials. The observed soliton parameters are not influenced by addition of the radiation, but the corresponding IST parameters must acquire specific shifts.

The appearance of these shifts can be traced back to the solution of the direct scattering problem. Indeed, the ZS system (5) has two different solutions $\Phi^{(s)}$ and $\Phi^{(sr)}$ characterized by the same discrete eigenvalue λ_n for the soliton-only and soliton-and-radiation potentials $\psi^{(s)}$ and $\psi^{(sr)}$, respectively. From definition of the right scattering problem (6) and (7), these solutions have the same asymptotic behavior at $x \rightarrow -\infty$, i.e., to the left of both the soliton and radiation. Then, both solutions should also coincide in the coordinate region between the soliton and radiation, far away from the radiation, since they propagate to this region through the same nonlinear structure—the soliton. On the other hand, to the right of the radiation, the solution $\Phi^{(sr)}$ must differ from the soliton-only case $\Phi^{(s)}$. The reflected wave at $x \rightarrow +\infty$ with the scattering coefficient $a \neq 0$ cannot appear due to presence of the soliton with eigenvalue λ_n , $a(\lambda_n) = 0$. However, since the function $a(\xi)$, $\xi \in \mathbb{R}e$, is now different in the presence of the radiation, it is continued differently to the upper half of the λ plane, that results in different complex derivative $a'(\lambda_n)$; and also the scattering coefficient $b(\lambda_n)$ may change as well. Both effects result in correction to the soliton norming constant ρ_n , see Eq. (9), and from where—to the IST position $x_n^{(IST)}$ and phase $\theta_n^{(IST)}$, see Eq. (11). The latter corrections are described by the following equations, see Refs. [50–53], connecting the observed soliton position $x_n^{(O)}$ and phase $\theta_n^{(O)}$ with the corresponding IST parameters $x_n^{(IST)}$ and $\theta_n^{(IST)}$:

$$x_n^{(O)} = x_n^{(IST)} + \Delta x_n^\pm, \quad (33)$$

$$\Delta x_n^\pm = -\frac{1}{2\pi} \int_{-\infty}^{\infty} H_{\mp(2\xi + \xi_n)} \frac{\ln[1 + |r(\xi)|^2]}{(\xi - \xi_n)^2 + \eta_n^2} d\xi,$$

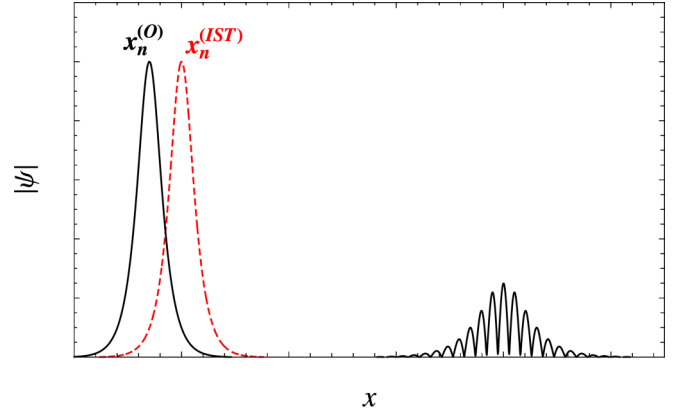


FIG. 1. Qualitative illustration of the difference between the observed $x_n^{(O)}$ and IST $x_n^{(IST)}$ positions of soliton in presence of localized nonlinear radiation. The solid black line shows the soliton-and-radiation potential, in which the soliton has the observed position $x_n^{(O)}$ and the IST position $x_n^{(IST)}$, while the dashed red line indicates single soliton reconstructed at $x_n^{(IST)}$.

$$\theta_n^{(O)} = \theta_n^{(IST)} + \Delta\theta_n^\pm, \quad (34)$$

$$\Delta\theta_n^\pm = -\frac{1}{\pi} \int_{-\infty}^{\infty} (\xi - \xi_n) H_{\mp(2\xi + \xi_n)} \times \frac{\ln[1 + |r(\xi)|^2]}{(\xi - \xi_n)^2 + \eta_n^2} d\xi.$$

Here Δx_n^\pm and $\Delta\theta_n^\pm$ correspond to corrections at $t \rightarrow \pm\infty$ due to presence of the radiation characterized with the reflection coefficient $r(\xi)$, while H stands for the Heaviside step function. The qualitative difference between the observed and IST positions is illustrated in Fig. 1.

Note that the IST position and phase change with time linearly as

$$x_n^{(IST)} = x_{n_0}^{(IST)} + V_n t, \quad (35)$$

$$\theta_n^{(IST)} = \theta_{n_0}^{(IST)} + \frac{1}{2}(A_n^2 + V_n^2)t,$$

where $x_{n_0}^{(IST)}$ and $\theta_{n_0}^{(IST)}$ are the corresponding parameters at $t = 0$, and $A_n = 2\eta_n$, $V_n = -2\xi_n$ are the soliton amplitude and group velocity; see Eqs. (10) and (11).

Let us now suppose that the IST position $x_n^{(IST)}$ and phase $\theta_n^{(IST)}$ of a soliton are calculated in presence of the nonlinear radiation, as in the case of the box potential (23), see the corresponding relation (32) for the soliton norming constants. Then, if we remove radiation from the scattering data, we must also remove the described above corrections, built into $x_n^{(IST)}$ and $\theta_n^{(IST)}$. Assuming that the observed position $x_n^{(O)}$ and phase $\theta_n^{(O)}$ must not change due to the removal procedure, we must renormalize the IST parameters as

$$\tilde{x}_n^{(IST)} = x_n^{(IST)} + \Delta x_n^\pm, \quad (35)$$

$$\tilde{\theta}_n^{(IST)} = \theta_n^{(IST)} + \Delta\theta_n^\pm, \quad (36)$$

where $\tilde{x}_n^{(\text{IST})}$ and $\tilde{\theta}_n^{(\text{IST})}$ are the renormalized space position and phase without the nonlinear radiation, while Δx_n^\pm and $\Delta \theta_n^\pm$ are given by Eqs. (33) and (34).

Equations (35) and (36) can be used to remove the nonlinear radiation if it is far away from the soliton, so the nonlinear structures practically do not interact in the physical space. However, removal of the radiation from the box potential (23) requires additional assumptions. Indeed, in this case the solitonic content and the radiation are both situated in the same region of space, and in addition to the renormalization shifts discussed above, there might be interaction shifts due to ongoing interaction between the soliton and radiation in the physical space. We consider the latter shifts in the following way.

Since the solitonic content of the box potential has zero velocities, see Eq. (29), we rewrite the asymptotic expressions (33) and (34) for the corrections Δx_n^\pm and $\Delta \theta_n^\pm$ to the limit of vanishing soliton velocity $\xi_n \rightarrow 0$:

$$\Delta x_n^\pm = -\frac{1}{4\pi} \int_{-\infty}^{\infty} \frac{\ln[1 + |r(\xi)|^2]}{\xi^2 + \eta_n^2} d\xi, \quad (37)$$

$$\Delta \theta_n^\pm = \pm \frac{1}{\pi} \int_0^{\infty} \frac{\xi \ln[1 + |r(\xi)|^2]}{\xi^2 + \eta_n^2} d\xi. \quad (38)$$

Here we have used that the absolute value of the reflection coefficient (26) is even function, $|r(\xi)| = |r(-\xi)|$. From Eq. (37), one can see that the position shift is the same before ($t \rightarrow -\infty$) and after ($t \rightarrow +\infty$) the collision of soliton with the nonlinear radiation, $\Delta x_n^- = \Delta x_n^+$; here we assume that the soliton has infinitesimally small positive velocity, so at some finite time it passes through the radiation. This allows us to suggest that the interaction shift of the soliton position is zero and the total position shift equals the renormalization shift only, $\Delta x_n = \Delta x_n^\pm$. The phase shift, on the other hand, changes its sign as the soliton passes through the radiation, $\Delta \theta_n^- = -\Delta \theta_n^+$. From this behavior, we assume that the total phase shift equals to the sum of the renormalization shift, $\Delta \theta_n^-$, and half of the full interaction shift, $(\Delta \theta_n^+ - \Delta \theta_n^-)/2$, i.e., it is simply zero, $\Delta \theta_n = 0$. In total, this yields the following correction to the soliton norming constants, see Eq. (11):

$$\tilde{\rho}_n = \rho_n e^{-\frac{\eta_n}{2\pi} \mathcal{I}_{N,n}}, \quad (39)$$

where $\mathcal{I}_{N,n}$ represents the integral

$$\mathcal{I}_{N,n} = \int_{-\infty}^{+\infty} \frac{\ln(1 + |r(\xi)|^2)}{\xi^2 + \eta_n^2} d\xi, \quad (40)$$

with η_n satisfying Eq. (29) and $r(\xi)$ given by Eq. (26).

Note that the general N -soliton variant of Eqs. (33) and (34) contains an additional term due to presence of other solitons, see Refs. [50,51]. Here we use the one-soliton formulas and apply the derived corrections to each of the N solitons individually, since, by removing only the continuous spectrum, we do not change the mutual soliton influence on their IST parameters.

The integral (40) for the box potential case can be analytically evaluated using the contour integration in the complex plane and the so-called Blaschke factors, leading to the fol-

lowing result:

$$\mathcal{I}_{N,n} = 2\pi L - \frac{2\pi}{\eta_n} \left\{ \ln \left[\frac{2\eta_n(1 + \eta_n L)}{1 - \eta_n^2} \right] + \ln \left[(-1)^{n-1} \prod_{j \neq n}^N \frac{\eta_n + \eta_j}{\eta_n - \eta_j} \right] \right\}, \quad (41)$$

see Appendix B and also Chap. I in monograph Ref. [39], where the similar integrals were considered. The dependency of the last term in Eq. (41) on the other solitons' eigenvalues comes from continuation of the integrand to the upper-half plane, where it has poles at the corresponding points.

Substituting Eqs. (32) and (41) into Eq. (39), we find the corrected IST norming constants:

$$\tilde{\rho}_n = 2i\eta_n(-1)^n \prod_{j \neq n}^N \frac{\eta_n + \eta_j}{\eta_n - \eta_j}. \quad (42)$$

Then, using the transformation (21), we obtain the corresponding corrected DM norming constants in the following simple form:

$$\tilde{C}_n = (-1)^n. \quad (43)$$

The eigenvalues (29) together with the norming constants (42) (for the IST formalism) or (43) (for the DM formalism) provide the complete set of the scattering data for the (reflectionless) solitonic model of the box potential. Note that Eq. (43) is consistent with the semiclassical approximation, asserting that real-valued single-humped wave field having a finite integral is characterized by the same norming constants, see, e.g., Ref. [35].

Also note that without correction of the norming constants (39), i.e., with the soliton parameters taken directly from Eqs. (29) and (32), the corresponding multisoliton solutions turn out to be nonsymmetric in the physical space with respect to mirror transformation $x \rightarrow -x$, as we discuss in Sec. VI and demonstrate in Appendix A. This asymmetry is removed after the norming constants are corrected, as described above.

V. SOLITONIC MODEL OF THE BOX POTENTIAL

A. Analytical properties

Let us consider the general properties of an N -soliton solution (N -SS) having the imaginary soliton eigenvalues $\lambda_n = i\eta_n$, $\eta_n \in \mathbb{R}$, and the DM norming constants that equal either plus or minus unity $C_n = (-1)^{\beta_n}$, $\beta_n \in \mathbb{N}$.

First, such a solution is real-valued, as can be easily verified with analysis of Eq. (20). Indeed, for $C_n = \pm 1$, the vectors $\tilde{\mathbf{q}}_n$ in Eq. (20) are either purely real or imaginary; additionally, each vector can be multiplied by an individual nonzero constant, since this constant is canceled anyway during division of the determinants. This means that we can always make all vectors $\tilde{\mathbf{q}}_n$ purely real, making the matrix elements M_{kj} purely imaginary, so the ratio of the two determinants is imaginary and the final result for the wave field is real.

Second, for the imaginary soliton eigenvalues and DM norming constants that equal unity in absolute value, $|C_n| = 1$, the N -SS is symmetric with respect to mirror transformation,

$\psi_{(N)}(-x) = \psi_{(N)}(x)$, which results in transposition of the matrices $\mathbf{M}(-x) = \mathbf{M}(x)^T$ and $\tilde{\mathbf{M}}(-x) = \tilde{\mathbf{M}}(x)^T$; see Eq. (20). Note that time dependency of the norming constants (19) changes their phases but not the absolute values, i.e., the symmetry $x \rightarrow -x$ is preserved during the evolution in time.

Third, in terms of the DM formalism, all the solitons for such a N -SS are located at the symmetry point $x = 0$ for all times, see Eq. (22); in particular, the imaginary soliton eigenvalues mean that such a solution is a bound state. For the corrected DM norming constants (43), the DM space positions and phases are written as

$$\tilde{x}_n^{(\text{DM})} = 0, \quad \tilde{\theta}_n^{(\text{DM})} = \frac{\pi}{2}[1 - (-1)^{n-1}]. \quad (44)$$

Interestingly, the largest soliton λ_1 always has zero phase, $\tilde{\theta}_1^{(\text{DM})} = 0$, and if we gradually increase the box width L so the number of solitons N in Eq. (28) increases, then each new soliton appears with the opposite phase compared to the previous one.

Finally, for $C_n = \pm 1$, the wave field at the symmetry point $x = 0$ can be found explicitly via the soliton eigenvalues [44]. For this purpose, we note that, at $x = 0$ and for each n , the matrices $\Phi^{(n)}$ and $\sigma^{(n)}$ in Eqs. (15)–(18) are real, symmetric, and have equal elements at their diagonals, while the vector \mathbf{q}_n has specific form

$$\Phi_{ml}^{(n)}(0, \lambda) \in \mathbb{R}, \quad \sigma_{ml}^{(n)}(0, \lambda) \in \mathbb{R}, \quad (45)$$

$$\Phi_{ml}^{(n)}(0, \lambda) = \Phi_{lm}^{(n)}(0, \lambda), \quad \sigma_{ml}^{(n)}(0, \lambda) = \sigma_{lm}^{(n)}(0, \lambda), \quad (46)$$

$$\Phi_{11}^{(n)}(0, \lambda) = \Phi_{22}^{(n)}(0, \lambda), \quad \sigma_{11}^{(n)}(0, \lambda) = \sigma_{22}^{(n)}(0, \lambda), \quad (47)$$

$$\mathbf{q}_n(0) = Q_n \begin{pmatrix} 1 \\ C_n \end{pmatrix}, \quad (48)$$

where Q_n is real parameter. Indeed, since all the eigenvalues are imaginary, $\lambda_n = i\eta_n$, $\eta_n \in \mathbb{R}$, then at the first step $n = 1$ we have

$$\begin{aligned} \Phi^{(0)}(0, \lambda) &= \mathbf{E}, \\ \mathbf{q}_1(0) &= \begin{pmatrix} 1 \\ C_1 \end{pmatrix}, \\ \sigma^{(1)}(0, \lambda) &= \mathbf{E} + \frac{\eta_1}{\eta - \eta_1} \begin{pmatrix} 1 & C_1 \\ C_1 & 1 \end{pmatrix}, \end{aligned}$$

where $\eta \in \mathbb{R}$ parameterizes the spectral parameter $\lambda = i\eta$ and \mathbf{E} is 2×2 unit matrix. Then, from Eqs. (16)–(18) and with $C_n = \pm 1$, it is easy to prove the properties (45)–(48) at each successive step of the recursive procedure.

The property (48) allows us to find the combination

$$\frac{q_{n1}^* q_{n2}}{|\mathbf{q}_n|^2} = \frac{C_n}{2}$$

in Eq. (15) and ultimately yields the wave field at the symmetry point:

$$\psi_{(N)}(0) = -2 \sum_{n=1}^N C_n \eta_n. \quad (49)$$

The discussed above analytical properties of the solitonic model are obtained from analysis of the determinant formula

(20) and the dressing procedures (15)–(18). Note that other ways to construct multisoliton solutions, such as the traditional IST formalism (12) and the Riemann-Hilbert problem approach [39], might turn out to be more convenient for analytical considerations, which we are going to explore in future studies.

B. Numerical results

Using the efficient numerical scheme for the DM developed previously in Ref. [24] in combination with 2000-digit precision arithmetic, we construct wave field $\psi_{(N)}(x)$ for the N -SS with the scattering data (29), (43), for the number of solitons ranging from $N = 32$ to 1024. In the numerical scheme, high-precision arithmetics is applied to accurately resolve large number of arithmetic operations with exponentially large and small numbers coming from the elements of vectors \mathbf{q}_n , see Eqs. (14)–(18). Though this inherent issue of the DM cannot be entirely avoided, the optimized algorithm developed in Ref. [54] (which wasn't used in the present paper) allows one to minimize the necessary numerical precision.

Note that, according to Eq. (30), for fixed number of solitons N , we may choose the parameter L describing the width of the box potential (23) differently. In this section, we choose $\Delta L = \pi/4$ in Eq. (30), that yields close to minimal residual oscillations, as well as close to minimal impact of the continuous spectrum on the integral characteristics of the wave field; the results for other choices of ΔL are qualitatively the same, as discussed in Appendix A.

As shown in Figs. 2(a) and 2(b), the constructed multisoliton solution resembles the box potential of the same width; in particular, it is purely real and positive, i.e., has the same complex phase as the condensate (the positivity is numerical observation for all choices of ΔL that we have tried). Oscillations of the wave field around unity shown in Figs. 2(a)–2(c) come from subtraction of the continuous spectrum from the box potential, i.e., appear due to reconstruction of the (box) potential having nonzero reflection coefficient with the reflectionless potential (multisoliton solution). At the edges, the oscillations resemble the well-known Gibbs phenomenon for reconstruction of a jump discontinuity with the Fourier transform. The amplitude of these oscillations is maximal at the edges, where it is close to 0.3, and decreases monotonically to the center of the box. Note that, at the edges, the amplitude varies moderately with parameter ΔL in Eq. (30), but does not change significantly with increasing number of solitons N ; see Figs. 2(a) and 2(b) and Appendix A. As we discuss in Appendix A, the similar oscillations are seen for the N -SS built from noncorrected norming constants, too.

In the central region, the amplitude of the oscillations decreases with increasing N as $\propto N^{-1/2}$, as demonstrated in Fig. 2(c) for several examples of the wave field and in Fig. 2(d) for the difference $|\psi_{(N)}(x) - 1|$ at $x = 0$ computed for N ranging from 32 to 8192. Interestingly, the period of the oscillations is close to π , Fig. 2(c), that corresponds to the shortest modulationally unstable mode $|k| = 2$, see Eq. (2), so, between the two absolute maximums at the edges, the total number of periods n_0 equals the number of solitons N minus one, $n_0 = N - 1$.

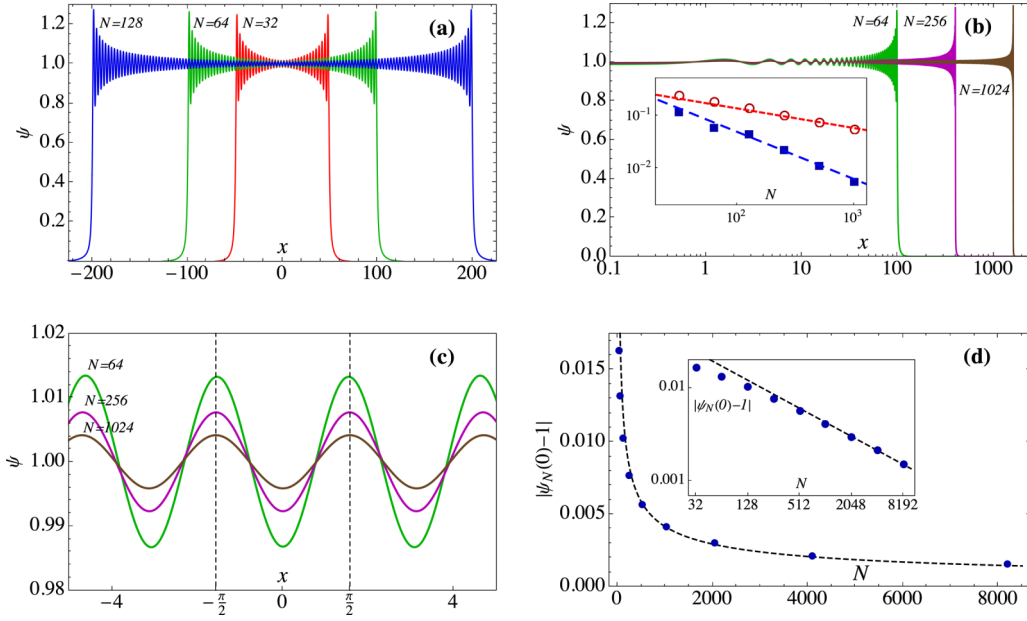


FIG. 2. (a)–(c) Wave field of the N -soliton solution (N -SS) for $N = 32$ (red), 64 (green), 128 (blue), 256 (purple), and 1024 (brown): (a) in linear scales, (b) in logarithmic horizontal scale, (c) in linear scales at the center of the box. Each N -SS curve is marked with the corresponding number of solitons. (d) Amplitude of the residual oscillations at the center $|\psi_{(N)}(0) - 1|$ as a function of N (blue points). The dashed black line indicates the fit $\propto N^{-1/2}$. The N -SS for all the figures are constructed from the scattering data (29) and (43) with $\Delta L = \pi/4$ in Eq. (30). The inset in panel (b) shows dependency of $(1 - L_s/L)$ (red circles) and $(1 - L_c/L)$ (blue squares) on N in double logarithmic scales, where L_s and L_c are defined according to Eqs. (50) and (51), respectively. The short-dashed red line indicates the fit $(1 - L_s/L) \propto N^{-\alpha_s}$ with $\alpha_s \approx 0.37$, while the long-dashed blue line—the fit $(1 - L_c/L) \propto N^{-\alpha_c}$ with $\alpha_c \approx 0.89$. The inset in panel (d) represents the same plot as in the main figure, but in double logarithmic scales.

Computing amplitude of the oscillations $\epsilon(x)$ at different sections $x = \varkappa L/2$ of the box with \varkappa ranging from 0 to 0.8 and for the number of solitons N from 32 to 1024, we observe the same convergence law to unity, $\epsilon(x) \propto N^{-1/2}$ for fixed \varkappa , see Appendix A. This leads us to the suggestion that the fraction of the box width L_s/L , within which the oscillations vanish with increasing number of solitons N , approaches unity as $N \rightarrow +\infty$. To test this hypothesis, we define L_s as length of the coordinate region $|x| \leq L_s/2$, where

$$|\psi_{(N)}(x) - 1| \leq |\psi_{(N)}(0) - 1| N^{1/4}. \quad (50)$$

Here the multiplier $N^{1/4}$ on the right-hand side (RHS) is taken arbitrarily, provided that with increasing N (i) it is growing and (ii) the whole RHS decreases. Taking into account that the wave field at the center approaches unity as $|\psi_{(N)}(0) - 1| \propto N^{-1/2}$, the particular choice $N^{1/4}$ leads to the RHS of the criterion (50) vanishing with increasing N as $N^{-1/4}$. As shown in the inset of Fig. 2(b), length L_s approaches box width L as $(1 - L_s/L) \propto N^{-\alpha_s}$ with $\alpha_s \approx 0.37$. Hence, we can conclude that the presented solitonic model (29), (43) approaches asymptotically to the condensate with increasing number of solitons N .

Note that the fraction of the box occupied by the pronounced edge oscillations decreases with increasing N , as can be seen directly from Figs. 2(a) and 2(b) for several examples of the multisoliton solution. In particular, length L_c of region $|x| \leq L_c/2$, where the oscillations are twice smaller than at the edges,

$$|\psi_{(N)}(x) - 1| \leq \epsilon_{\max}/2, \quad (51)$$

approaches the box width L as $(1 - L_c/L) \propto N^{-\alpha_c}$ with $\alpha_c \approx 0.89$, see the inset of Fig. 2(b). Here, the amplitude at the edges is defined as maximum of the wave field minus unity, $\epsilon_{\max} = \max |\psi_{(N)}(x)| - 1$.

VI. DISCUSSION

By analogy with the Gibbs phenomenon, the presence of the edge oscillations with finite amplitude in Figs. 2(a) and 2(b) might be explained by the jump discontinuity of the box potential at $x = \pm L/2$, which is not resolved adequately when reconstructing the wave field with solitons only. If this suggestion is true, then the oscillations might be significantly decreased when an appropriate smoothing is applied at the box edges. One way to verify this conjecture would be to construct a solitonic model of a smoothed box-shaped potential, for instance, using the numerical tools developed in Refs. [55,56]; currently, we leave this line of research for future studies. Note that, as was demonstrated for the semiclassical approximation in Ref. [57], any smoothing, no matter how small, has a leading order effect on the time evolution of the potential. The other way is to consider another analytically solvable case of the potential without discontinuities, for instance, the hyperbolic secant potential $\psi(x) = \text{sech}(x/L)$.

In Appendix C, we study the latter case using the same techniques as discussed previously and arrive at exactly the same corrected DM norming constants (43). For different values of the parameter L , the constructed wave field turns out to be very similar to the original sech-potential one, and the residual oscillations, present for noninteger L (otherwise,

the sech-potential is a pure N -SS with $N = L$), vanish with increasing N in the entire coordinate space. Note that our conjecture that the edge oscillations can be significantly diminished for a potential with smooth edges is also consistent with the semiclassical approximation, stating that a smooth large wave field can be approximated by solitons [35].

As shown in the previous section for the box potential (23), and also in Appendix C for the sech potential, the constructed solitonic models are symmetric with respect to mirror transformation $x \rightarrow -x$, as well as the original wave fields. Meanwhile, both the corrected IST soliton parameters (that correspond to the solitonic models) and the noncorrected IST parameters (that together with the nonlinear radiation correspond to the original wave fields) do not show this symmetry. Indeed, the IST space positions are connected with the norming constants as $x_n^{(IST)} = \ln(|\rho_n|/2\eta_n)/2\eta_n$, see Eq. (11), so for the box potential case the corrected positions are positive for all the solitons, $\tilde{x}_n^{(IST)} > 0$, due to the inequality $|\tilde{\rho}_n|/2\eta_n = |\prod_{j \neq n}^N \frac{\eta_n + \eta_j}{\eta_n - \eta_j}| > 1$, see Eq. (42). And since the noncorrected norming constants are connected with the corrected ones as

$$\rho_n = \tilde{\rho}_n e^{\frac{\eta_n}{2\pi} \mathcal{I}_{N,n}},$$

and the integral $\mathcal{I}_{N,n}$ is positive, see Eqs. (39) and (40), the noncorrected space positions are positive as well, $x_n^{(IST)} > 0$. The same inequalities are valid for the sech-potential when L is noninteger, for both the corrected and noncorrected IST space positions.

This asymmetry in IST space positions observed for the symmetric wave fields comes from the nonsymmetric formulation of the scattering problem (6) and (7). In contrast to the IST formalism, the DM does not have such left-right asymmetry in its construction [43,45], and the DM space positions turn out to be symmetric, $x_n^{(DM)} = 0$. Note that we cannot find the DM norming constants corresponding to the box potential (23) that contains both solitons and nonlinear radiation, since, from the one hand, there are no developed methods that would allow us to solve the direct scattering problem to the DM scattering data directly, and, on the other hand, Eq. (21) connecting the IST and DM norming constants is valid only when the nonlinear radiation is absent.

Meanwhile, if we build N -SS from the noncorrected IST norming constants (32) by calculating the DM norming constants via Eq. (21),

$$C'_n = -\frac{2\eta_n(1 + \eta_n L)}{e^{\eta_n L}(1 - \eta_n^2)} \prod_{j \neq n}^N \frac{\eta_n + \eta_j}{\eta_n - \eta_j} \equiv \tilde{C}_n e^{-\frac{\eta_n}{2\pi} \mathcal{I}_{N,n}}, \quad (52)$$

and then applying the dressing procedure, we arrive to nonsymmetric DM space positions and nonsymmetric wave field. Indeed, in Eq. (52) we have $\mathcal{I}_{N,n} > 0$ and $|\tilde{C}_n| = 1$, so the corresponding DM space positions are negative for all the solitons, $x_n^{(DM)} < 0$, for both the box potential and the sech-potential (when L is noninteger) cases. The resulting wave fields turn out to be nonsymmetric, see Appendices A and C.

Note that, in the DM formalism, the location of all solitons at the symmetry point $x = 0$ for both solitonic models should follow from the symmetry considerations. Indeed, the original wave fields are symmetric, so the solitonic models are expected to be symmetric as well. Then, in the symmetric

formalism of the DM, the solitons should have symmetric positions. Since all the soliton eigenvalues are different, this is only possible when all the solitons are located at $x = 0$.

In the present paper, the box potential is considered at a single moment of time $t = 0$; meanwhile, its time evolution represents an important problem called the dam break. Due to the presence of the continuous spectrum for any box length L , the analytical consideration of this evolution within the IST approach is problematic, that led to broad application of approximation techniques and numerical methods, see, e.g., Refs. [35,41,58,59]. In our approach, we completely neglect the nonlinear radiation content of the wave field that allows us to examine N -soliton description of the wave field at any moment. Leaving this for further studies, we highlight the question of comparing our N -soliton model with the models of the dam break problem mentioned above.

VII. CONCLUSIONS

In the present paper, we have introduced an IST-based approach to the studies of strongly nonlinear wave fields, that consists of construction of their purely solitonic models. In particular, on the examples of the box potential and the sech potential, we have found specific corrections to the soliton norming constants that arise due to removal of the continuous spectrum and constructed their solitonic models that approach asymptotically to the original wave fields at large number of solitons. We think that the developed technique can be applied for other symmetric wave fields governed by various integrable partial differential equations, in particular, using the scattering data found numerically [55,56] or in the semiclassical approximation [60]. For nonsymmetric wave fields, the solitons may have nonzero velocities and the absolute value of the reflection coefficient may not be an even function, so the interaction shifts discussed in Sec. IV may not be as easily assumed.

We believe that the proposed approach will benefit the studies of various nonlinear phenomena that occur in strongly nonlinear wave fields. For instance, the constructed solitonic model of the condensate can be used to investigate the modulational instability [4,21,26,61] and the dam break problems [27,41,58,59,62]. Another possible application is related to the theory of rogue waves on the condensate background, see, e.g., Refs. [2,5,6] and also the recent theoretical and experimental studies where the typical spatiotemporal profiles of the rogue waves were interpreted as a result of soliton interactions [24,63,64].

ACKNOWLEDGMENTS

The authors thank participants of Prof. V.E. Zakharov's seminar "Nonlinear Waves" and, especially, Gennady El and Vladimir Zakharov for fruitful discussions. The work on correction of the norming constants reported in Sec. IV was supported by the Russian Science Foundation (Grant No. 19-72-30028 to A.G. and D.A.). The work on the hyperbolic secant potential reported in Appendix C was supported by the Russian Science Foundation (Grant No. 20-71-00022 to A.G.). The work of P.S. and S.R. was supported by the Agence Nationale de la Recherche through the I-

SITE ULNE (ANR-16-IDEX-0004), the LABEX CEMPI (ANR-11-LABX-0007), and the Equipex Flux (ANR-11-EQPX-0017), as well as by the Ministry of Higher Education and Research, Hauts de France council and European Regional Development Fund (ERDF) through the CPER project Photonics for Society (P4S). Simulations were performed at the Novosibirsk Supercomputer Center (NSU).

APPENDIX A: WAVE FIELD FOR THE SOLITONIC MODEL OF THE BOX POTENTIAL

In the main part of the paper, we have presented the solitonic model of the box potential characterized by the eigenvalues λ_n (29) and the corrected norming constants $\tilde{\rho}_n$ (42)—for the IST formalism, or \tilde{C}_n (43)—for the DM formalism. The eigenvalues λ_n depend on width L of the box potential, which is parameterized as $L = L_N + \Delta L$, where L_N and ΔL are given by Eq. (30). The presented wave fields have been computed for the parameter $\Delta L = \pi/4$, which yields close to minimal residual oscillations. In this Appendix, we examine the constructed wave fields in more detail and consider different modifications of the scattering data for the solitonic model.

First, we demonstrate convergence of the solitonic model to the condensate in a broad region of the box when the number of solitons N increases. For this purpose, using the parameter $\Delta L = \pi/4$ in Eq. (30) and increasing N from 32 to 1024, we compute amplitude of the oscillations $\epsilon(x)$ around the condensate at different sections of the box $x = \varkappa L/2$ with \varkappa ranging from 0 to 0.8 and discover that, for fixed \varkappa , the oscillations vanish as $\epsilon(x) \propto N^{-1/2}$, see Fig. 3. The amplitude is calculated as maximum deviation from the condensate $\epsilon(x) = \max_{y \in \Theta} |\psi_{(N)}(y) - 1|$ over the oscillation period π centered at $x = \varkappa L/2$, $\Theta = [\varkappa L/2 - \pi/2, \varkappa L/2 + \pi/2]$. This result has lead us to suggest the criterion (50) for the length L_s of the coordinate region $|x| \leq L_s/2$ where the oscillations vanish with increasing N and, as has been discussed in Sec. V, this length L_s approaches the whole box L by power law as $N \rightarrow +\infty$.

Second, we consider how the solitonic model is changed when the exact formula for the eigenvalues (29) is replaced

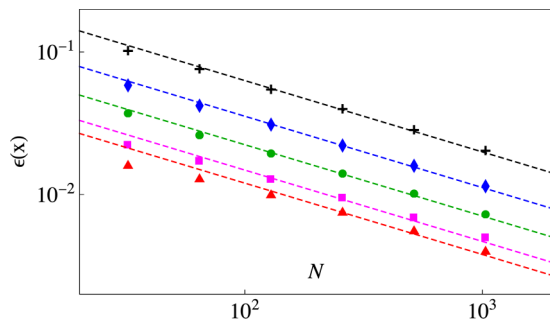


FIG. 3. Amplitude of the oscillations $\epsilon(x)$ at different sections of the box $x = \varkappa L/2$ versus the number of solitons N , for $\varkappa = 0$ (red triangles), 0.2 (magenta squares), 0.4 (green dots), 0.6 (blue diamonds), and 0.8 (black crosses); note the double logarithmic scales. The dashed lines show the fits $\propto N^{-1/2}$. The amplitude $\epsilon(x)$ is calculated for the N -SS constructed from the scattering data (29) and (43) with $\Delta L = \pi/4$ in Eq. (30).

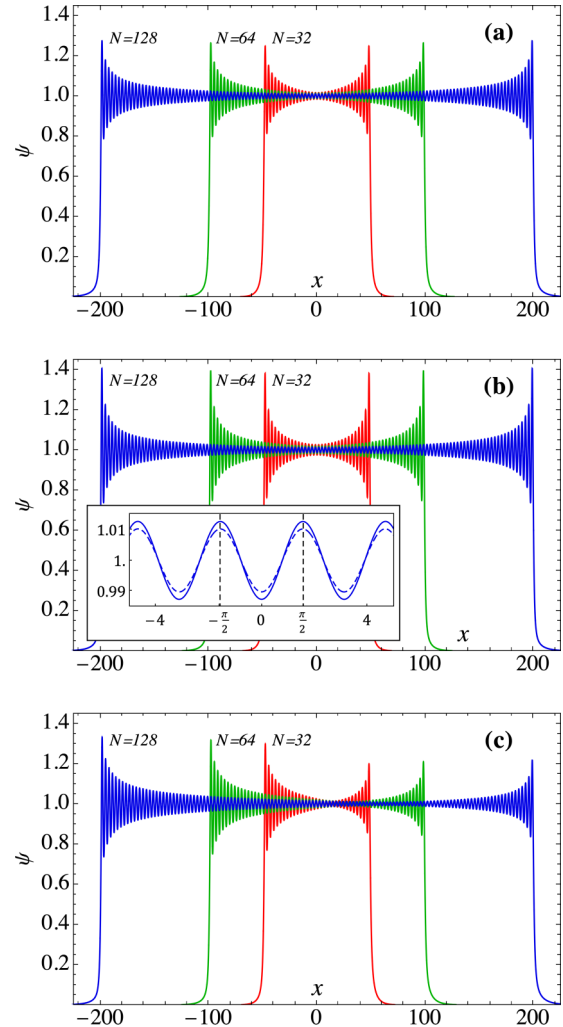


FIG. 4. Wave fields of N -SS for $N = 32$ (red), 64 (green), and 128 (blue), constructed from (a) the box eigenvalues λ_n (29) and the corrected DM norming constants \tilde{C}_n (43), (b) the semiclassical box eigenvalues $\lambda_n^{(sc)}$ (31) and the corrected DM norming constants \tilde{C}_n , and (c) the box eigenvalues λ_n and the noncorrected DM norming constants C_n (52). Each N -SS curve is marked with the corresponding number of solitons. The parameter ΔL in Eq. (30) is the same for all cases, $\Delta L = \pi/4$. The panel (a) coincides with Fig. 2(a). The inset in panel (b) shows two 128-SS at the center of the box: constructed from the box eigenvalues λ_n (dashed line) and from the semiclassical eigenvalues $\lambda_n^{(sc)}$ (solid line).

by the semiclassical one (31). In this test, the DM norming constants are taken according to Eq. (43) that corresponds to all the solitons located at the symmetry point $x = 0$ with alternating phases of zero and π , see Eq. (44), and the parameter ΔL in Eq. (30) is fixed to $\pi/4$. As shown in Fig. 4(b), the usage of the semiclassical eigenvalues leads to from slightly (at the center) to moderately (at the edges) elevated residual oscillations compared to the exact eigenvalues, see also Fig. 4(a).

Third, we examine the N -SS built without correction of the norming constants, i.e., using the noncorrected IST norming constants (32) corresponding to DM norming constants (52). The result is demonstrated in Fig. 4(c) for $N = 32, 64$, and

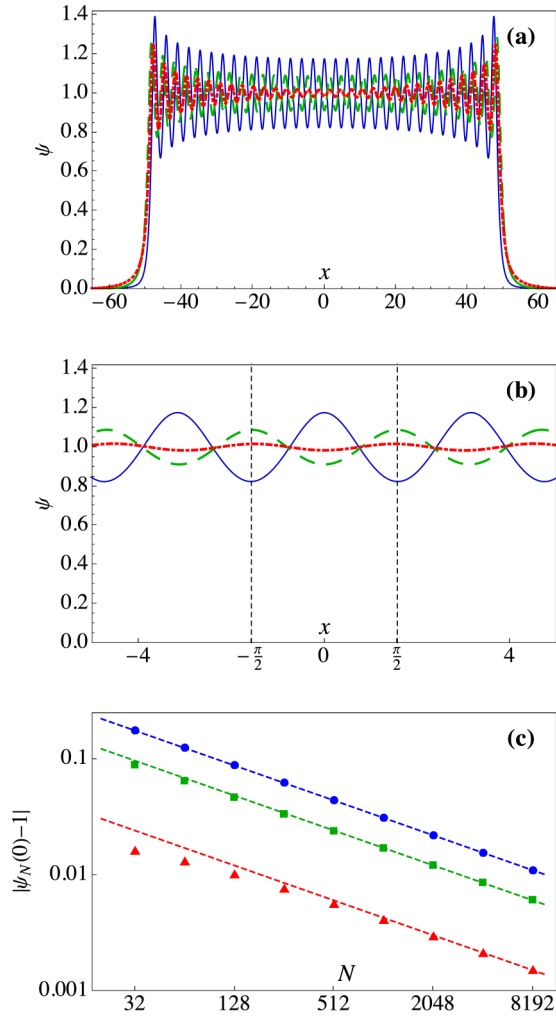


FIG. 5. The N -SS constructed from the scattering data (29) and (43) for different values of the parameter ΔL in Eq. (30). (a) The general form of the 32-SS, for $\Delta L = 0$ (solid blue), $\pi/4$ (dash-dotted red), and $\pi/2$ (dashed green). (b) The same solutions at the center of the box. (c) Amplitude of the oscillations at the center, $|\psi_{(N)}(0) - 1|$, versus the number of solitons N (points), in double logarithmic scales. The blue circles mark the case $\Delta L = 0$, the red triangles $-\pi/4$, and the green squares $-\pi/2$. The dashed lines indicate the fits $\propto N^{-1/2}$.

128; the eigenvalues λ_n are given by the transcendental equation (29) and the parameter ΔL equals $\pi/4$. As one can see, the wave fields turn out to be nonsymmetric with enhanced oscillations at their left sides. Note that the norming constants (52) correspond to negative DM space positions for all the solitons, $x_n^{(\text{DM})} < 0$, see Sec. VI.

Finally, we examine influence of the parameter ΔL on the solitonic model defined by the eigenvalues λ_n (29) and the corrected norming constants \tilde{C}_n (43). In Figs. 5(a) and 5(b), we demonstrate 32-SS constructed for three different values of this parameter: $\Delta L = 0$, $\pi/4$, and $\pi/2$. Note that Eq. (29) determining λ_n is transcendental, and for its numerical solution at $\Delta L = 0$ we have used small nonzero value of 10^{-4} order for ΔL , avoiding the indeterminate expression which appears for the root $\lambda_n = 0$. As shown in the figures, among the three examples, the cases $\Delta L = 0$ and $\pi/4$ are characterized

by the strongest and weakest oscillations, respectively. The oscillation period is very close to π for all three cases. At the center of the box, the amplitude of the oscillations vanishes with increasing N as $|\psi_{(N)}(0) - 1| \propto N^{-1/2}$, see Fig. 5(c).

Repeating the convergence study discussed in the beginning of this Appendix, but now for the parameter $\Delta L = 0$ corresponding to the strongest oscillations, we observe the same asymptotic behavior for the oscillation amplitude $\epsilon(x) \propto N^{-1/2}$ at different sections $x = \varkappa L/2$ of the box from $\varkappa = 0$ to 0.8, and the same power-law convergence $(1 - L_s/L) \propto N^{-\alpha_s}$ with $\alpha_s \approx 0.43$ for the length L_s of the coordinate region (50) where the oscillations vanish with increasing N . We have checked that other values of ΔL yield the similar results.

We conclude that, irrespective of the specific choice of parameter ΔL , our solitonic model of the box potential has the same basic properties that have been discussed in Sec. V on the example of the case $\Delta L = \pi/4$, namely, the N -SS built according to our model are purely real and symmetric, the amplitude of the residual oscillations is maximal at the edges, where it is close to 0.3, and minimal at the center of the box, where it vanishes with increasing number of solitons N as $\propto N^{-1/2}$, while the region L_s , where the oscillations are vanishing with increasing N , approaches asymptotically to the whole box, $L_s \rightarrow L$, as $N \rightarrow +\infty$.

The residual oscillations are minimal—both at the edges and at the center of the box—for the parameter ΔL close to $\pi/4$. This is demonstrated in Figs. 6(a) and 6(b), where the oscillation amplitude at the edges ϵ_{max} and at the center ϵ_{min} is shown for ΔL changing continuously from 0 to π , for 32-SS, 64-SS, and 128-SS. At the edges, the amplitude is calculated as the maximum of the wave field minus unity, $\epsilon_{\text{max}} = \max |\psi_{(N)}(x)| - 1$, while at the center—as maximum deviation from the condensate $\epsilon_{\text{min}} = \max_{x \in \Theta} |\psi_{(N)}(x) - 1|$ over the oscillation period $\Theta = [-\pi/2, \pi/2]$ centered at $x = 0$. Note that the minimal edge oscillations are achieved for ΔL slightly larger than $\pi/4$, while the minimal center oscillations for ΔL slightly smaller than $\pi/4$.

The oscillations are maximal for $\Delta L = 0$, i.e., at the point when a new soliton appears, see Eq. (29). Using the semiclassical formula (31) for approximate calculations, one can easily get that the two smallest eigenvalues for the $\Delta L = 0$ case are located at $\lambda_N^{(0)} = 0$ and $\lambda_{N-1}^{(0)} \approx i\sqrt{2/N}$, while the smallest eigenvalue for the $\Delta L = \pi/4$ case—at $\lambda_N^{(\pi/4)} \approx i/\sqrt{2N}$, that is, at the center of the interval $[\lambda_N^{(0)}, \lambda_{N-1}^{(0)}]$. In this sense, we think that the maximal oscillations at $\Delta L = 0$ can be interpreted as a result of the new soliton appearance, while the minimal oscillations at close to $\Delta L = \pi/4$ as the midpoint between the two emerging soliton events at $L = L_N$ and $L = L_N + \pi$; see the discussion on soliton emergence in Ref. [65].

The changes in the oscillations' strength with increasing box width L resemble the behavior of the box continuous spectrum content. The relative impact of the nonlinear radiation can be examined through the first integral of motion—the wave action,

$$\mathcal{I}_1 = \int_{-\infty}^{\infty} |\psi|^2 dx, \quad (\text{A1})$$

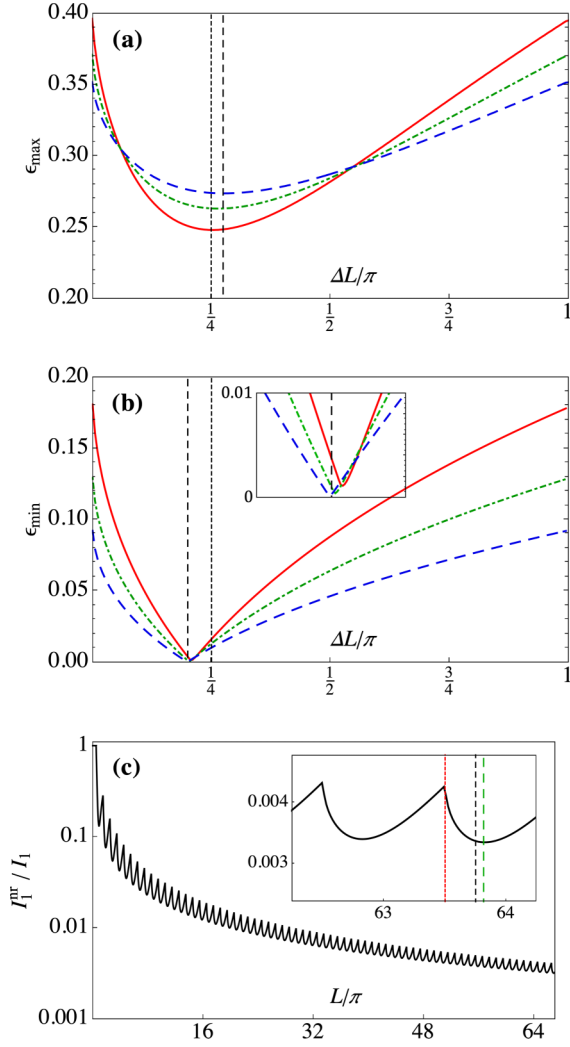


FIG. 6. (a), (b) Amplitude of the oscillations (a) at the edges ϵ_{\max} and (b) at the center ϵ_{\min} versus the parameter ΔL in Eq. (30), for 32-SS (solid red), 64-SS (dash-dotted green), and 128-SS (dashed blue). The short-dashed vertical lines indicate $\Delta L = \pi/4$, while the long-dashed vertical lines mark the minima of the 128-SS curves. The inset in panel (b) shows zoom near the minimum. (c) Ratio $\mathcal{I}_1^{(nr)}/\mathcal{I}_1$ between wave actions of the nonlinear radiation $\mathcal{I}_1^{(nr)}$ (A2) and the box potential \mathcal{I}_1 , as a function of L in semilogarithmic scales. The inset shows zoom near $N = 64$; the short-dashed red and dashed black lines indicate $\Delta L = 0$ and $\pi/4$, while the long-dashed green line marks the local minimum of the presented curve. The N -SS for all the figures are constructed from the scattering data (29) and (43).

which for the box potential (23) equals $\mathcal{I}_1 = L$ and for the solitonic model can be found directly via soliton eigenvalues (29) as $\mathcal{I}_1^{(sm)} = 4 \sum_{j=1}^N \eta_j$, see, e.g., Ref. [10]. This allows us to find wave action for the nonlinear radiation,

$$\mathcal{I}_1^{(nr)} = \mathcal{I}_1 - \mathcal{I}_1^{(sm)} = L - 4 \sum_{j=1}^N \eta_k; \quad (\text{A2})$$

the ratio $\mathcal{I}_1^{(nr)}/\mathcal{I}_1$ is shown in Fig. 6(c) as a function of L . For $L < \pi/2$, the solitonic content is absent, see Eq. (28), and the ratio equals to unity. For large L , the impact of the nonlin-

ear radiation decreases close to exponentially in accordance with the semiclassical IST theory [10]; however, pronounced oscillations with period π around the exponential trend are visible and the function $\mathcal{I}_1^{(nr)}/\mathcal{I}_1$ takes local maximums at $L = L_N$, i.e., at the points when a new soliton appears. The local minima are located near the points corresponding to $\Delta L = \pi/4$, as shown in the inset of Fig. 6(c).

APPENDIX B: CALCULATION OF THE INTEGRAL $\mathcal{I}_{N,n}$

In this Appendix, we present calculation of the integral $\mathcal{I}_{N,n}$, which defines corrections to the soliton norming constants; see Eqs. (39) and (40).

Using the property of the scattering coefficients $|a(\xi)|^2 + |b(\xi)|^2 = 1$, $\xi \in \mathbb{R}$, together with definition of the reflection coefficient $r = b/a$, see Eqs. (8) and (9), we rewrite the original integral as

$$\begin{aligned} \mathcal{I}_{N,n} &= \int_{-\infty}^{+\infty} \frac{\ln[1 + |r(\xi)|^2]}{\xi^2 + \eta_n^2} d\xi \\ &= - \int_{-\infty}^{+\infty} \frac{\ln[|a(\xi)|^2]}{\xi^2 + \eta_n^2} d\xi, \end{aligned} \quad (\text{B1})$$

where, for the box potential,

$$a(\xi) = e^{iL\xi} \left\{ \cos(\chi L) - i\xi \frac{\sin(\chi L)}{\chi} \right\}, \quad (\text{B2})$$

$$\chi = \sqrt{1 + \xi^2}. \quad (\text{B3})$$

The square modulus in the integral (B1) can be represented as product $|a(\xi)|^2 = a_u(\xi) \cdot a_l(\xi)$, $\xi \in \mathbb{R}$, of the two functions,

$$a_{u,l}(\xi) = \cos(L\chi) \mp i\xi \sin(L\chi)/\chi, \quad (\text{B4})$$

where the sign minus corresponds to a_u and the sign plus to a_l . Then, using the relation $a_u(\xi) = a_l(-\xi)$ valid for real ξ , we can further rewrite the integral as

$$\begin{aligned} \mathcal{I}_{N,n} &= - \int_{-\infty}^{+\infty} \frac{\ln[a_u(\xi)]}{\xi^2 + \eta_n^2} d\xi - \int_{-\infty}^{+\infty} \frac{\ln[a_l(\xi)]}{\xi^2 + \eta_n^2} d\xi \\ &= -2 \int_{-\infty}^{+\infty} \frac{\ln[a_u(\xi)]}{\xi^2 + \eta_n^2} d\xi = -2\mathcal{I}_a. \end{aligned} \quad (\text{B5})$$

Being analytically continued to the upper half-plane, the function a_u has N roots, which coincide with the eigenvalues λ_n of the box potential and are defined by Eq. (29), see Refs. [47–49]. Similarly, being continued to the lower half-plane, the function a_l has the same N roots, but mirrored with respect to the real axis. Note that, being analytically continued to the whole complex plane, both functions a_u and a_l have additional roots in the lower and upper half-planes, respectively.

The presence of roots under the logarithm in Eq. (B5) doesn't allow for straightforward contour integration in the complex plane. To overcome this difficulty, we multiply the function a_u by the so-called Blaschke factors, similarly to what is done in Ref. [39],

$$\tilde{a}_u(\xi) = a_u(\xi) \times \prod_{j=1}^N \frac{\xi + i\eta_j}{\xi - i\eta_j}, \quad (\text{B6})$$

where $\lambda_j = i\eta_j$, $j = 1, \dots, N$, are the eigenvalues of the box potential.

On the one hand, multiplication by the Blaschke factors [i.e., replacement of a_u by \tilde{a}_u in Eq. (B5)] doesn't change the integral $\mathcal{I}_{N,n}$, since integration of each Blaschke factor alone yields zero:

$$\int_{-\infty}^{+\infty} \frac{d\xi}{\xi^2 + \eta_n^2} \ln \left[\frac{\xi + i\eta_j}{\xi - i\eta_j} \right] = 0. \quad (\text{B7})$$

On the other hand, the new function \tilde{a}_u has no roots in the upper half-plane and, after the replacement, the integral

$$\mathcal{I}_a = \int_{-\infty}^{+\infty} \frac{\ln[\tilde{a}_u(\xi)]}{\xi^2 + \eta_n^2} d\xi \quad (\text{B8})$$

can be readily taken.

Indeed, using the Cauchy's integral theorem and the classical contour of integration which runs along the real axis from minus to plus infinity and then returns back via the infinite semi-circle in the upper half-plane, we get

$$\mathcal{I}_a + \mathcal{I}_{a\infty} = (2\pi i) \operatorname{Res}_{\lambda=i\eta_n} \left(\frac{\ln[\tilde{a}_u(\lambda)]}{\lambda^2 + \eta_n^2} \right), \quad (\text{B9})$$

where $\mathcal{I}_{a\infty}$ is the integral over the semicircle and Res stands for residue. The residue appears at the only pole $\lambda = i\eta_n$ due to denominator of the integrand. The integral over the infinite semicircle can be found using the polar coordinates in the complex plane, $\lambda = R e^{i\phi}$, and the approximation

$$\tilde{a}_u(\lambda) \approx a_u(\lambda) \approx \cos(L\chi) - i \sin(L\chi) \approx e^{-iL\lambda},$$

valid for $|\lambda| \gg 1$, so

$$\mathcal{I}_{a\infty} = \int_0^\pi \frac{-iLR e^{i\phi}}{R^2 e^{2i\phi}} R e^{i\phi} i d\phi = \pi L. \quad (\text{B10})$$

As for the residue, we have

$$(2\pi i) \operatorname{Res}_{\lambda=i\eta_n} \left(\frac{\ln[\tilde{a}_u(\lambda)]}{\lambda^2 + \eta_n^2} \right) = \frac{\pi}{\eta_n} \left\{ \sum_{j \neq n}^N \ln \left[\frac{i\eta_n + i\eta_j}{i\eta_n - i\eta_j} \right] + \ln [2i\eta_n a'_u(i\eta_n)] \right\}, \quad (\text{B11})$$

where the second term containing the derivative a'_u appears as a result of indeterminate expression $a_u/(\lambda - i\eta_n)$ at $\lambda = i\eta_n$; recall that $a_u(i\eta_n) = 0$.

To find the derivative, it is instructive first to rewrite the condition $a(\lambda_n) = 0$ on the eigenvalues λ_n of the box potential,

$$\cos(\chi_n L) - i\lambda_n \frac{\sin(\chi_n L)}{\chi_n} = 0, \quad (\text{B12})$$

where $\chi_n = \sqrt{1 + \lambda_n^2}$, see Eqs. (B2) and (B3), to the form

$$\sin(\chi_n L) = \Omega_n \chi_n, \quad \Omega_n = \pm 1. \quad (\text{B13})$$

In this relation, each eigenvalue λ_n is characterized by the specific sign Ω_n which depends on index n .

Then, calculating the derivative a'_u straightforwardly and using Eq. (B12) once again to relate the sine and cosine in the process, we arrive to

$$a'_u(i\eta_n) = -i\Omega_n \frac{1 + \eta_n L}{1 - \eta_n^2}. \quad (\text{B14})$$

This allows us to get the integral \mathcal{I}_a , and via it, the full integral $\mathcal{I}_{N,n}$,

$$\mathcal{I}_{N,n} = 2\pi L - \frac{2\pi}{\eta_n} \left\{ \ln \left[\frac{2\eta_n(1 + \eta_n L)}{1 - \eta_n^2} \right] + \ln \left[\Omega_n \prod_{j \neq n}^N \frac{\eta_n + \eta_j}{\eta_n - \eta_j} \right] \right\}. \quad (\text{B15})$$

To find the sign Ω_n , we note that the argument of the second logarithm in Eq. (B15) must be positive, since the argument of the first logarithm is positive and the whole integral (B1) is positively defined (in particular, it is always real). The product

$$\prod_{j \neq n}^N \frac{\eta_n + \eta_j}{\eta_n - \eta_j}$$

changes its sign with each change of the index n by unity, and is positive for $n = 1$, since in this case the largest root is η_1 . Then,

$$\Omega_n = (-1)^{n-1},$$

that leads us to the final result (41).

APPENDIX C: SOLITONIC MODEL FOR THE HYPERBOLIC SECANT POTENTIAL

Similarly to the main part of the paper, in this Appendix we construct a solitonic model for the hyperbolic secant potential,

$$\psi(x) = \operatorname{sech}(x/L), \quad (\text{C1})$$

where parameter L represents its characteristic width.

The scattering problem for this potential was solved in Ref. [66] to the scattering coefficients

$$a(\xi) = \frac{\Gamma^2_{-i\xi L + \frac{1}{2}}}{\Gamma_{-i\xi L + \frac{1}{2} + L} \Gamma_{-i\xi L + \frac{1}{2} - L}}, \quad (\text{C2})$$

$$b(\xi) = -\frac{\sin(\pi L)}{\cosh(\pi L \xi)}, \quad (\text{C3})$$

where Γ is the Eulergamma function. The soliton eigenvalues, defined from the condition $a(\lambda) = 0$, lie on the imaginary axis,

$$\lambda_n = i\eta_n = i \left[1 - \frac{n - \frac{1}{2}}{L} \right], \quad n = 1, \dots, N, \quad (\text{C4})$$

where $N = \text{Integer}[L + \frac{1}{2}]$. The latter means that, similarly to Eq. (30), the width L can be parameterized as

$$L = L_N + \Delta L, \quad L_N = N - \frac{1}{2}, \quad \Delta L \in [0, 1), \quad (\text{C5})$$

meaning that, for increasing L , the number of solitons N remains constant until the next jump by one soliton at $L = L_N + 1$. The (noncorrected) IST norming constants can be found via the definition (9),

$$\rho_n = -\frac{i \Gamma_{1+2L-n}}{L(n-1)! \Gamma_{1+L-n}^2}, \quad (\text{C6})$$

though the calculation is not trivial—see Ref. [67] for details.

Note that, for integer L , the potential (C1) is reflectionless, $r = b/a = 0$, see Eq. (C3), i.e., it contains only solitons. In

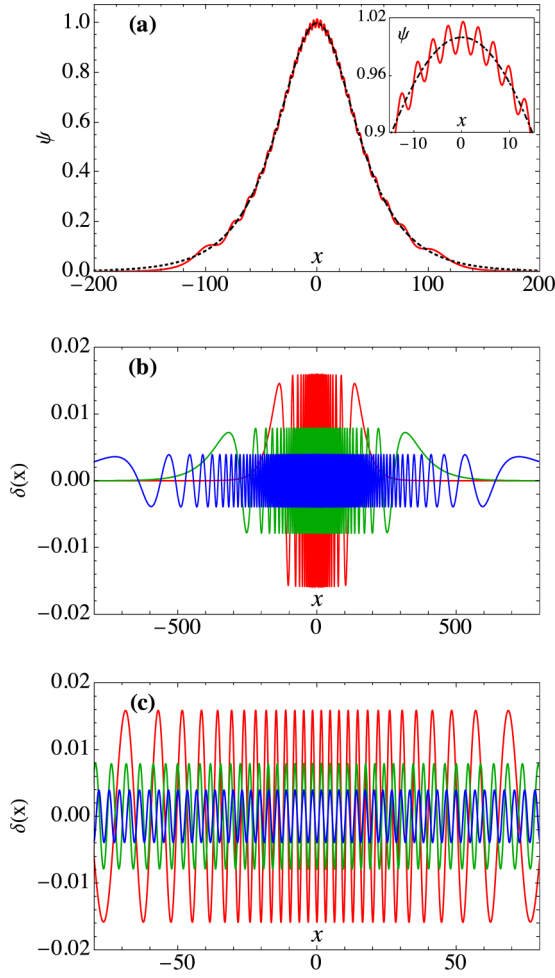


FIG. 7. (a) Wave field of N -SS (solid red line) constructed from the scattering data (C4), (C9), for $N = 32$ and $\Delta L = 0$ in Eq. (C5). The original sech-potential (C1) is shown with the dashed black line. The inset shows zoom near the symmetry point $x = 0$. (b) Difference $\delta(x) = \text{sech}(x/L) - \psi_{(N)}(x)$ between the sech potential and its solitonic model, for $N = 32$ (red, reaches the largest maximum amplitude in the figure), 64 (green, the intermediate maximum amplitude), and 128 (blue, the smallest maximum amplitude); the parameter $\Delta L = 0$ corresponds to the maximum oscillations. (c) Zoom of the above panel demonstrating varying oscillation period.

this case, that corresponds to the parameter $\Delta L = 1/2$ in Eq. (C5), the nonlinear radiation and (therefore) the residual oscillations are both absent. To construct the solitonic model for the general case of noninteger L , one needs to find the corrected norming constants via Eqs. (39) and (40). These equations are applicable, because the solitonic content of the sech potential has zero velocities, see Eq. (C4), and the absolute value of the reflection coefficient $|r| = |b/a|$ is even function since $b(\xi)$ and $|a(\xi)|$ are both even, see Eqs. (C2) and (C3) (here we use the well-known property of the gamma function $\Gamma(z^*) = \Gamma(z)^*$, i.e., $|\Gamma(z^*)| = |\Gamma(z)|$).

Calculation of the integral $\mathcal{I}_{N,n}$ defining the corrections to the soliton norming constants goes through the same steps as for the box potential case. In particular, we represent the square modulus in the integral (B1) as product $|a(\xi)|^2 = a_u(\xi) \cdot a_l(\xi)$, $\xi \in \mathbb{R}$, of the two functions $a_u(\xi) = a(\xi)$ and

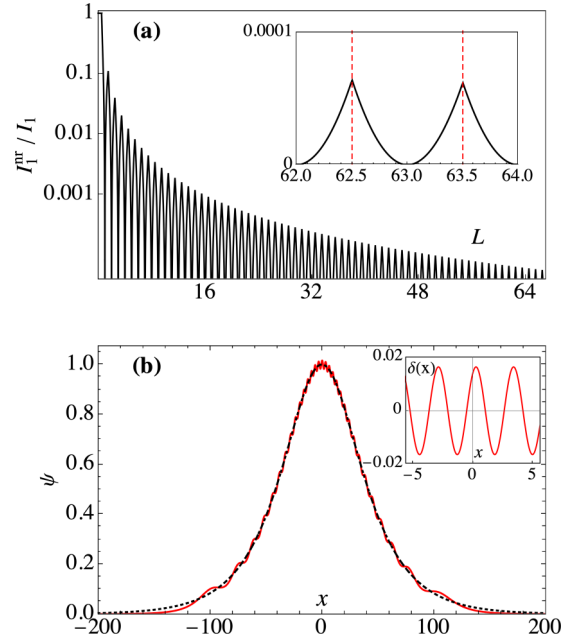


FIG. 8. (a) Ratio $\mathcal{I}_1^{(nr)}/\mathcal{I}_1$ between wave actions of the nonlinear radiation $\mathcal{I}_1^{(nr)}$ (A2) and the sech-potential \mathcal{I}_1 as a function of L in semilogarithmic scales. The inset shows zoom near $N = 64$; the dashed red lines indicate $\Delta L = 0$. (b) Wave field of N -SS (solid red line) constructed from the eigenvalues (C4) and the noncorrected IST norming constants (C6) using transition to the DM formalism via Eq. (21), for $N = 32$ and $\Delta L = 0$ in Eq. (C5). The original sech-potential (C1) is shown with the dashed black line. The inset shows the nonsymmetry of the difference $\delta(x) = \text{sech}(x/L) - \psi_{(N)}(x)$ with respect to the mirror transformation $x \rightarrow -x$.

$a_l(\xi) = a(\xi)^* = a(-\xi)$, and then calculate the integral \mathcal{I}_a , see Eq. (B5), by continuing the function $a_u(\xi)$ to the upper half-plane with replacement $\xi \rightarrow \lambda$ and using the Blaschke factors (B6). As a result, we arrive to Eq. (B9), in which the integral over the infinite semicircle vanishes, since for $|\lambda| \rightarrow +\infty$ we have $a_u(\lambda) \rightarrow 1$, see, e.g., Ref. [10], and therefore $\tilde{a}_u(\lambda) \rightarrow 1$. To calculate the residue (B11), we use the well-known property of the gamma function,

$$\text{Res}_{z=-n} \Gamma_z = \frac{(-1)^n}{n!},$$

that ultimately leads us to

$$\begin{aligned} \mathcal{I}_{N,n} &= -\frac{2\pi}{\eta_n} \left\{ \ln \left[\frac{(-1)^{n-1} (n-1)! (2L-2n+1) \Gamma_{1+L-n}^2}{\Gamma_{1+2L-n}} \right] \right. \\ &\quad \left. + \ln \left[\prod_{j \neq n}^N \frac{\eta_n + \eta_j}{\eta_n - \eta_j} \right] \right\}. \end{aligned} \quad (C7)$$

Using the latter result and Eq. (C6), we find the corrected IST norming constants,

$$\tilde{\rho}_n = \rho_n e^{-\frac{\eta_n}{2\pi} \mathcal{I}_{N,n}} = 2i\eta_n (-1)^n \prod_{j \neq n}^N \frac{\eta_n + \eta_j}{\eta_n - \eta_j}, \quad (C8)$$

and, via Eq. (21), the corrected DM norming constants,

$$\tilde{C}_n = (-1)^n, \quad (\text{C9})$$

which coincide with those for the box potential case.

The multisoliton solution constructed from the scattering data (C4), (C9) has all the same properties as discussed in the beginning of Sec. V, namely, it is real valued and symmetric with respect to mirror transformation $x \rightarrow -x$; all of its solitons have DM space positions at the symmetry point $x = 0$ and DM phases of zero and π , see Eq. (44), while the wave field at $x = 0$ can be calculated via Eq. (49).

Computing this N -SS numerically for different values of parameter L , we observe that it is very similar to the original sech potential, having small residual oscillations on the hyperbolic secant background for noninteger L , see Fig. 7(a). In contrast to the box potential case, these oscillations have constant amplitude in space, but their period increases when moving from the center to the edges, as demonstrated in Figs. 7(b) and 7(c). The oscillation amplitude decreases with

increasing number of solitons as $\propto N^{-1}$, and, for the symmetry point $x = 0$, this relation is proved analytically by substituting (C4) into (49), that yields

$$\psi_{(N)}(0) = 1 \mp \frac{\Delta L - \frac{1}{2}}{N + \Delta L - \frac{1}{2}}, \quad (\text{C10})$$

where the sign minus corresponds to even N , and the sign plus, to odd N .

The oscillation amplitude is maximal at $\Delta L = 0$, i.e., at the point when a new soliton appears, and minimal at $\Delta L = 1/2$, when the sech potential represents an exact multisoliton solution. The ratio $\mathcal{I}_1^{(\text{nr})}/\mathcal{I}_1$ between wave actions of the nonlinear radiation $\mathcal{I}_1^{(\text{nr})}$ (A2) and the sech-potential \mathcal{I}_1 takes local maximums at $\Delta L = 0$ and local minimums (coinciding with zero) at $\Delta L = 1/2$, see Fig. 8(a). The N -SS constructed without correction of the norming constants, i.e., from the noncorrected IST norming constants (C6) via transition (21) to the DM formalism, turns out to be nonsymmetric, see Fig. 8(b), with all the solitons having negative DM space positions, $x_n^{(\text{DM})} < 0$, as has been discussed in Sec. VI.

-
- [1] Y. S. Kivshar and G. Agrawal, *Optical Solitons: From Fibers to Photonic Crystals* (Academic Press, New York, 2003).
- [2] C. Kharif, E. Pelinovsky, and A. Slunyaev, *Rogue Waves in the Ocean, Observation, Theories and Modeling*, Advances in Geophysical and Environmental Mechanics and Mathematics Series (Springer, Heidelberg, 2009).
- [3] A. Osborne, *Nonlinear Ocean Waves* (Academic Press, New York, 2010).
- [4] V. E. Zakharov and L. Ostrovsky, *Physica D* **238**, 540 (2009).
- [5] N. Akhmediev, J. M. Soto-Crespo, and A. Ankiewicz, *Phys. Rev. A* **80**, 043818 (2009).
- [6] N. Akhmediev, A. Ankiewicz, and J. M. Soto-Crespo, *Phys. Rev. E* **80**, 026601 (2009).
- [7] T. B. Benjamin and J. E. Feir, *J. Fluid Mech.* **27**, 417 (1967).
- [8] V. E. Zakharov, *J. Appl. Mech. Tech. Phys.* **9**, 190 (1968).
- [9] V. E. Zakharov and A. B. Shabat, *Sov. Phys. JETP* **34**, 62 (1972).
- [10] S. Novikov, S. V. Manakov, L. P. Pitaevskii, and V. E. Zakharov, *Theory of Solitons: The Inverse Scattering Method* (Springer Science & Business Media, New York, 1984).
- [11] M. J. Ablowitz and H. Segur, *Solitons and the Inverse Scattering Transform* (SIAM, Philadelphia, 1981), Vol. 4.
- [12] S. K. Turitsyn and S. A. Derevyanko, *Phys. Rev. A* **78**, 063819 (2008).
- [13] S. Derevyanko and E. Small, *Phys. Rev. A* **85**, 053816 (2012).
- [14] S. Randoux, P. Suret, A. Chabchoub, B. Kibler, and G. El, *Phys. Rev. E* **98**, 022219 (2018).
- [15] A. Slunyaev, *Eur. J. Mech. B* **25**, 621 (2006).
- [16] A. Slunyaev, *Radiophys. Quantum Electron.* **61**, 1 (2018).
- [17] P. Suret, A. Tikan, F. Bonnefoy, F. Copie, G. Ducrozet, A. Gelash, G. Prabhudesai, G. Michel, A. Cazaubiel, E. Falcon, G. El, and S. Randoux, *Phys. Rev. Lett.* **125**, 264101 (2020).
- [18] V. E. Zakharov, *Stud. Appl. Math.* **122**, 219 (2009).
- [19] S. Randoux, P. Walczak, M. Onorato, and P. Suret, *Phys. Rev. Lett.* **113**, 113902 (2014).
- [20] P. Walczak, S. Randoux, and P. Suret, *Phys. Rev. Lett.* **114**, 143903 (2015).
- [21] D. S. Agafontsev and V. E. Zakharov, *Nonlinearity* **28**, 2791 (2015).
- [22] D. S. Agafontsev and V. E. Zakharov, *Nonlinearity* **29**, 3551 (2016).
- [23] J. M. Soto-Crespo, N. Devine, and N. Akhmediev, *Phys. Rev. Lett.* **116**, 103901 (2016).
- [24] A. A. Gelash and D. S. Agafontsev, *Phys. Rev. E* **98**, 042210 (2018).
- [25] A. E. Kraych, P. Suret, G. El, and S. Randoux, *Phys. Rev. Lett.* **122**, 054101 (2019).
- [26] A. Gelash, D. Agafontsev, V. Zakharov, G. El, S. Randoux, and P. Suret, *Phys. Rev. Lett.* **123**, 234102 (2019).
- [27] F. Bonnefoy, A. Tikan, F. Copie, P. Suret, G. Ducrozet, G. Prabhudesai, G. Michel, A. Cazaubiel, E. Falcon, G. El, and S. Randoux, *Phys. Rev. Fluids* **5**, 034802 (2020).
- [28] S. V. Manakov, *Sov. Phys. JETP* **38**, 693 (1974).
- [29] E. N. Pelinovsky, E. G. Shurgalina, A. V. Sergeeva, T. G. Talipova, G. A. El, and R. H. J. Grimshaw, *Phys. Lett. A* **377**, 272 (2013).
- [30] V. Karpman and V. Solov'ev, *Physica D* **3**, 487 (1981).
- [31] Y. S. Kivshar and B. A. Malomed, *Rev. Mod. Phys.* **61**, 763 (1989).
- [32] V. S. Gerdjikov, I. M. Uzunov, E. G. Evstatiev, and G. L. Diankov, *Phys. Rev. E* **55**, 6039 (1997).
- [33] V. Gerdjikov and I. Uzunov, *Physica D* **152**, 355 (2001).
- [34] V. Gerdjikov, M. D. Todorov, and A. Kyuldjiev, *Math. Comput. Simul.* **121**, 166 (2016).
- [35] S. Kamvissis, K. D.-R. McLaughlin, and P. D. Miller, *Semiclassical Soliton Ensembles for the Focusing Nonlinear Schrödinger Equation* (Annals of Mathematics Studies, Princeton University Press, Princeton, 2003), Vol. 154.
- [36] L. D. Landau and E. M. Lifshitz, *Quantum Mechanics: Non-relativistic Theory. V. 3 of Course of Theoretical Physics* (Pergamon Press New York, Oxford, 1958).

- [37] G. L. Lamb, *Elements of Soliton Theory* (Wiley-Interscience, New York, 1980).
- [38] X. Zhou, *Commun. Pure Appl. Math.* **42**, 895 (1989).
- [39] L. D. Faddeev and L. A. Takhtajan, *Hamiltonian Methods in the Theory of Solitons* (Springer Science & Business Media, Berlin, 2007).
- [40] Z. Lewis, *Phys. Lett. A* **112**, 99 (1985).
- [41] R. Jenkins and K. D. T.-R. McLaughlin, *Commun. Pure Appl. Math.* **67**, 246 (2014).
- [42] A. Gelash and R. Mullyadzhano, *Phys. Rev. E* **101**, 052206 (2020).
- [43] V. E. Zakharov and A. V. Mikhailov, *Sov. Phys. JETP* **47**, 1017 (1978).
- [44] N. N. Akhmediev and N. V. Mitzkevich, *IEEE J. Quantum Electron.* **27**, 849 (1991).
- [45] V. B. Matveev and M. A. Salle, *Darboux Transformations and Solitons* (Springer-Verlag, Berlin, 1991).
- [46] V. Aref, [arXiv:1605.06328](https://arxiv.org/abs/1605.06328).
- [47] M. Klaus and J. K. Shaw, *Phys. Rev. E* **65**, 036607 (2002).
- [48] E. N. Tsoy and F. K. Abdullaev, *Phys. Rev. E* **67**, 056610 (2003).
- [49] M. Desaix, D. Anderson, L. Helczynski, and M. Lisak, *Phys. Rev. Lett.* **90**, 013901 (2003).
- [50] L. Martinez Alonso, *Phys. Rev. Lett.* **54**, 499 (1985).
- [51] L. Martinez Alonso, *Phys. Rev. D* **32**, 1459 (1985).
- [52] E. Kuznetsov, A. Mikhailov, and I. Shimokhin, *Physica D* **87**, 201 (1995).
- [53] M. Borghese, R. Jenkins, and K. D.-R. McLaughlin, *Annales de Inst. H. Poincaré C, Analyse Nonlinéaire* **35**, 887 (2018).
- [54] P. J. Prins and S. Wahls, *Commun. Nonlinear Sci. Numer. Simul.* **102**, 105782 (2021).
- [55] R. Mullyadzhano and A. Gelash, *Opt. Lett.* **44**, 5298 (2019).
- [56] R. I. Mullyadzhano and A. A. Gelash, *Radiophys. Quantum Electron.* **63**, 786 (2021).
- [57] M. G. Forest and K.-R. McLaughlin, *J. Nonlinear Science* **7**, 43 (1998).
- [58] A. Kamchatnov, A. Gammal, F. K. Abdullaev, and R. A. Kraenkel, *Phys. Lett. A* **319**, 406 (2003).
- [59] G. A. El, E. G. Khamis, and A. Tovbis, *Nonlinearity* **29**, 2798 (2016).
- [60] A. Tovbis and S. Venakides, *Physica D* **146**, 150 (2000).
- [61] A. E. Kraych, D. Agafontsev, S. Randoux, and P. Suret, *Phys. Rev. Lett.* **123**, 093902 (2019).
- [62] G. Xu, M. Conforti, A. Kudlinski, A. Mussot, and S. Trillo, *Phys. Rev. Lett.* **118**, 254101 (2017).
- [63] D. Agafontsev and A. Gelash, *Front. Phys.* **9**, 610896 (2021).
- [64] A. Chabchoub, A. Slunyaev, N. Hoffmann, F. Dias, B. Kibler, G. Genty, J. Dudley, and N. Akhmediev, *Front. Phys.* **9**, 633549 (2021).
- [65] R. Mullyadzhano and A. Gelash, *Phys. Rev. Lett.* **126**, 234101 (2021).
- [66] J. Satsuma and N. Yajima, *Prog. Theor. Phys. Suppl.* **55**, 284 (1974).
- [67] A. I. Maimistov and A. M. Basharov, *Nonlinear Optical Waves*, Vol. 104 (Kluwer Academic Publishers, Dordrecht, Boston, London, 1999).